Target Positioning Accuracy of V2X Sidelink Joint Communication and Sensing

Caterina Giovannetti, *Graduate Student Member, IEEE*, Nicolò Decarli, *Member, IEEE*, Stefania Bartoletti, *Member, IEEE*, Richard A. Stirling-Gallacher, *Member, IEEE*, and Barbara M. Masini, *Senior Member, IEEE*

***Abstract*—Joint communication and sensing (JCS) is gaining popularity in vehicular scenarios for detecting and localizing nearby objects or other vehicles using vehicle-to-everything (V2X) communications, thus complementing or improving on-board sensors. Despite the numerous benefits, V2X communications, particularly in sidelink, suffer from inter-vehicle interference. In this letter, we evaluate the impact of physical and radio access communication parameters on device-free positioning based on JCS with sidelink V2X. We focus on estimating range, angle, and location in the presence of multi-user interference.**

***Index Terms*—Joint communication and sensing, 5G NR-V2X, V2X sidelink, radar sensing, position error bound.**

I. Introduction

VEHICLE-TO-EVERYTHING (V2X) communications allow vehicles to exchange information with other vehicles, other road users, and the infrastructure. In particular, the exchange of information gathered by on-board sensors such as RADAR, cameras, and LiDAR leads to the understanding of the driving environment, thus increasing roads' efficiency and safety.

Joint communication and sensing (JCS) arises as a new opportunity to complement these technologies, as it provides sensing functionalities *for free* by exploiting the same signal already employed for V2X communication. This could be extremely beneficial in terms of saving hardware and spectrum resources since it is no longer necessary to embed new components. JCS is gaining popularity also because, differently from on-board sensors that are typically based on proprietary solutions, it relies on standard technologies, e.g., 5G [1], [2], [3]. In addition, it overcomes the limitations of these sensors caused, for example, by visibility impairments.

Manuscript received 25 September 2023; revised 23 November 2023; accepted 20 December 2023. Date of publication 25 December 2023; date of current version 8 March 2024. This work was supported by the WiLab-Huawei Joint Innovation Center. The associate editor coordinating the review of this article and approving it for publication was B. Tan. *(Corresponding author: Caterina Giovannetti.)*

Caterina Giovannetti is with the National Research Council, IEIIT, 40136 Bologna, Italy, and also with WiLab-CNIT, 40136 Bologna, Italy, and also with the DEI, University of Bologna, 40136 Bologna, Italy (e-mail: caterina.giovannetti@ieiit.cnr.it).

Nicolò Decarli and Barbara M. Masini are with the National Research Council, IEIIT, 40136 Bologna, Italy, and also with WiLab-CNIT, 40133 Bologna, Italy (e-mail: nicolo.decarli@ieiit.cnr.it; barbara.masini@ieiit.cnr.it).

Stefania Bartoletti is with the DIE, University of Rome Tor Vergata, 00133 Rome, Italy, and also with WiLab-CNIT, 00133 Rome, Italy (e-mail: stefania.bartoletti@uniroma2.it).

Richard A. Stirling-Gallacher is with the Munich Research Center, Huawei Technologies Duesseldorf GmbH, 80992 Munich, Germany (e-mail: richard.sg@huawei.com).

Digital Object Identifier 10.1109/LWC.2023.3346937

In the context of V2X, recent works show how sidelink measurements (e.g., angle estimation or ranging) represent a huge opportunity for device-based positioning, thanks to the smaller path loss between nearby UEs (compared with the downlink path loss), lower latency, as well as the possibility to use distributed antennas or arrays [4], [5], [6], [7]. However, sidelink communication signals can be also leveraged for device-free sensing and positioning, i.e., detection, ranging, and localization of other vehicles or obstacles without relying on any devices, yet using signal reflections. In particular, considering the vehicle as a monostatic RADAR, localization of a passive target can use multiple antennas to obtain angular and range measurements, and localize an object in proximity. In this sense, device-free localization can be used also to complement or improve active positioning systems e.g., sidelink-based and network-based active positioning, sensors, or GNSS, which may be limited due to obstructions or other factors.

The vast majority of research efforts so far have been concerned with solutions that are not expressly intended for vehicular wireless access technologies, and they rarely target the intelligent transport system (ITS) band, namely the communication systems around the carrier frequency of 5.9 GHz thought for vehicular applications [1], [2], [3], [5], [8]. In addition, there are no specific works that deal with the use of sidelink V2X for device-free sensing and positioning. More recently, in [9], the authors proposed a model to evaluate the impact of radio access parameters on the range and Doppler estimation performance, yet without considering bearing information and position estimation, while in [10] also the bearing estimation is taken into account, but in a V2I scenario where the sensing procedure is thought to enhance communication.

In this letter, we evaluate the target positioning accuracy limits for device-free positioning considering 5G-V2X JCS. We consider range and bearing estimation, in the presence of multi-user interference. In fact, one of the main challenges when dealing with V2X sidelink signals is the presence of inter-vehicle interference, as spectrum resources might be autonomously allocated by vehicles. Moreover, we characterize target localization by considering the combined effect of range and bearing estimation. To this end, the Cramér-Rao lower bound (CRLB) for the parameters of interest is considered as performance benchmark. Results show that, in the presence of inter-vehicle interference, system-level parameters such as modulation and coding scheme (MCS), subcarrier spacing (SCS) and packet size affect the sensing and localization performance in a different way with respect to the interference-free case. The presented framework and results can drive the design of JCS schemes for device-free positioning considering V2X sidelink communication signals.

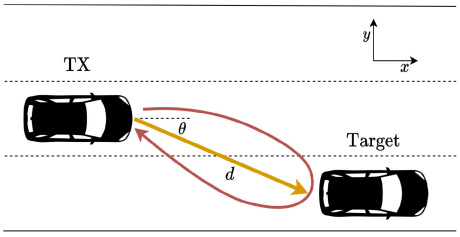

Fig. 1. Example scenario: a vehicle transmits a packet using 5G NR-V2X sidelink and aims at localizing a passive target from the analysis of the received echo.

II. Localization Accuracy Limits

We consider a vehicle that transmits data packets through 5G NR-V2X signals and jointly aims at detecting and localizing passive targets in its surroundings thanks to RADAR processing of the backscattered signal response. The transmitting vehicle operates as a monostatic RADAR, i.e., with the RADAR receiver co-located with the transmitter. In this way and by assuming a full duplex architecture, transmitted data symbols are known and can be considered as pilots for the sake of RADAR sensing [9], [11], [12].

With reference to Fig. 1, we consider a transmitting vehicle located at $(x,\, y) = (0,\, 0)$ and a generic target at distance d from the vehicle, with angle θ (clockwise) with respect to its direction. Thus, adopting a polar coordinate system with respect to the vehicle, the target location to be estimated can be denoted as $\mathbf{p} = [\theta, d]^\top$. For further convenience, we define as $\tilde{\mathbf{p}} = [x, y]^\top$ the Cartesian equivalent of the position $\mathbf{p}$, i.e., $d = \sqrt{x^2 + y^2}$ and $\theta = \arctan y/x$.

The 5G NR-V2X sidelink exploits the cyclic prefix orthogonal frequency-division multiplexing (OFDM) signal to convey information, hence the generic complex transmitted symbol can be expressed as

$$s_m(t) = \sum_{n=0}^{N-1} \sqrt{P_{nm}} x_{nm} e^{\mathrm{j}2\pi n \Delta f t} \operatorname{rect}\left(\frac{t - m T_{\mathrm{sym}}}{T_{\mathrm{sym}}}\right) \quad (1)$$

where P_{nm} is the power allocated to the n-th subcarrier of the m-th symbol and x_{nm} is the information content transmitted in the n-th subcarrier of the m-th symbol. The transmission of a data packet spans M OFDM symbols and N subcarriers. The symbol time $T_{\mathrm{sym}} = T + T_{\mathrm{cp}}$ includes the duration of the cyclic prefix T_{cp} and $T = 1/\Delta f$, in which Δf is the SCS. The transmitting vehicle sends the band-pass version of the sidelink signal (1) modulated at frequency f_{c} to perform JCS. To enable angle of arrival (AoA) estimation, we assume that the vehicle is equipped with a sensing receiver fitted with a uniform linear array (ULA) composed of N_{ant} antennas. In fact, despite standard V2X transceivers conceived for vehicular communications at the FR1 (i.e., sub-6 GHz) are usually single-antenna devices, sensing-based localization can leverage the adoption of multiple antennas to combine angle and range estimates to locate the target [13].

Considering a point target located at $\mathbf{p} = [\theta, d]^\top$ from the vehicle reference system, moving with relative velocity v, it is possible to write the received signal as

$$y_{nmk} = \sqrt{P_{nm}}\, x_{nm}\, T\, h_{nmk} \times e^{-\mathrm{j}2\pi n \Delta f \tau} e^{\mathrm{j}2\pi f_c \nu m T_{\mathrm{sym}}} e^{\mathrm{j}\pi k \sin\theta} + z_{nmk} \quad (2)$$

for $n = 0, 1, \ldots, N-1$, $m = 0, 1, \ldots, M-1$, and $k = 0, 1, \ldots, N_{\mathrm{ant}} - 1$, where h_{nmk} is the channel amplitude coefficient, and we accounted for a half-wavelength ULA at the receiver, resulting in a signal impinging from the target which produces a linear phase shift along the different antennas. The term z_{nmk} is the additive white Gaussian noise (AWGN), with $z_{nmk} \sim \mathcal{CN}(0, \sigma_{\mathrm{n}}^2)$. The first and second exponential terms express the phase shifts introduced by the propagation delay $\tau = 2d/c$ and the Doppler shift $\nu = 2 f_{\mathrm{c}} v/c$, where c is the speed of light. By processing the MNN_{ant} samples, the RADAR receiver aims at obtaining the estimate $\widehat{\mathbf{p}} = [\widehat{\theta}, \widehat{d}]$ of $\mathbf{p} = [\theta, d]$.

Considering the OFDM signal structure in (2), range estimation is carried out by looking at the phase shift produced on the received data symbols along the different subcarriers by the signal backscattered by the target at distance d. The accuracy limit for range estimation is given by the CRLB, which is the theoretical minimum variance of any unbiased estimator of the considered parameter and denotes therefore the best achievable performance [14]. The CRLB for the range estimation is given by [15]

$$\mathsf{CRLB}^{\left(\hat{d}\right)} = \frac{3c^2}{8\pi^2 MNN_{\mathrm{ant}}\, \mathsf{SINR} (N^2 - 1)\Delta f^2} \quad (3)$$

where SINR is the signal to interference plus noise ratio (SINR). In particular, since V2X communications are severely limited by interference [16], we account the degradation coming from both noise of power P_{n} and interference of power I with the SINR given by $\mathsf{SINR} = P_{\mathrm{R}}/(P_{\mathrm{n}} + I)$. The received power P_{R} is given by the RADAR equation

$$P_{\mathrm{R}} = P_{\mathrm{T}} \frac{G^2 c^2 \sigma}{(4\pi)^3 f_{\mathrm{c}}^2 d^4} \quad (4)$$

where P_{T} is the power transmitted by the source vehicle, G is the antenna element gain and σ is the RADAR cross section (RCS), which quantifies how detectable an object is by RADAR. The SINR considers not only noise power $P_{\mathrm{n}} = k_{\mathrm{B}} T_0 F N \Delta f$, being k_{B} the Boltzmann constant, T_0 the reference temperature and F the noise figure, but also the effect of interference I caused by vehicles transmitting in the same time slot and with overlapped resources, that can become significant as the number of vehicles in the scenario increases, as highlighted in [9]. Note that in (3) a processing gain N_{ant} coming from the exploitation of the N_{ant} receiving antennas is present, differently from traditional expressions [15], [17], [18]. Indeed, thanks to the independence of the noise samples at the different antenna ports, the N_{ant} receiving antennas provide additional information to be exploited for range estimation.

Considering the ULA at the RADAR receiver, the bearing estimation can be carried out by looking at the phase shift for each subcarrier and OFDM symbol along the N_{ant} antennas. The CRLB for the bearing estimation is given by [14]

$$\mathsf{CRLB}^{\left(\hat{\theta}\right)} = \frac{6}{\pi^2 MNN_{\mathrm{ant}}\, \mathsf{SINR} \left(N_{\mathrm{ant}}^2 - 1\right) \cos^2\theta} \quad (5)$$

where we considered an inter-element spacing of $\lambda/2$, with $\lambda = c/f_{\mathrm{c}}$. Note that in (5) a processing gain MN is obtained, since MN independent observations can be collected to obtain bearing estimates. By comparing (3) and (5), we can observe that the CRLB for range estimation improves rapidly as the number of subcarriers N increases (larger bandwidth thus better time resolution), whereas the CRLB for bearing estimation improves as the number of antennas N_{ant} increases (larger

array aperture thus better angular resolution). In addition, despite the CRLB for range estimation is independent on the range (except for the intrinsic dependence on the SINR), the CRLB for bearing estimation depends on the angle θ itself; in particular, bearing estimation accuracy is maximum for $\theta = 0$, while estimation is not possible for $\theta = \pm\pi/2$.

Depending on the position $\mathbf{p}$, both range and bearing estimates impact the positioning accuracy; in fact, a given error on the bearing produces a larger positioning error as the distance d increases. To account for this phenomenon, we compute the position error bound (PEB), i.e., the bound on the positioning accuracy, which allows us to provide a quantitative evaluation of the positioning performance limit of JCS based on sidelink 5G NR-V2X. Specifically, the PEB is defined as [19]

$$\mathsf{PEB} = \sqrt{\mathrm{tr}\left(\tilde{\mathbf{J}}^{-1}(\tilde{\mathbf{p}})\right)} \tag{6}$$

where $\tilde{\mathbf{J}}(\tilde{\mathbf{p}})$ is the Fisher information matrix (FIM) of the target position estimate $\tilde{\mathbf{p}}$ expressed in Cartesian coordinates. From the CRLB expressions for range and bearing estimation, respectively in (3) and (5), it is possible to derive the FIM $\tilde{\mathbf{J}}(\tilde{\mathbf{p}})$ by considering the polar to Cartesian conversion according to

$$\tilde{\mathbf{J}}(\tilde{\mathbf{p}}) = \mathbf{C}^{\top}(\mathbf{p})\,\mathbf{J}(\mathbf{p})\,\mathbf{C}(\mathbf{p}) \tag{7}$$

where $\mathbf{C}(\mathbf{p})$ is the Jacobian matrix defined as

$$\mathbf{C}(\mathbf{p}) = \begin{bmatrix} -\frac{\sin\theta}{d} & \frac{\cos\theta}{d} \\ \cos\theta & \sin\theta \end{bmatrix} \tag{8}$$

and the FIM for bearing and range estimates $\mathbf{J}(\mathbf{p})$ is

$$\mathbf{J}(\mathbf{p}) = \begin{bmatrix} \frac{1}{\mathsf{CRLB}^{(\hat{\theta})}} & 0 \\ 0 & \frac{1}{\mathsf{CRLB}^{(\hat{d})}} \end{bmatrix}. \tag{9}$$

After some algebraic manipulation, we obtain

$$\tilde{\mathbf{J}}(\tilde{\mathbf{p}}) = \begin{bmatrix} \frac{\sin^2\theta}{d^2\mathcal{B}} + \frac{\cos^2\theta}{\mathcal{R}} & -\frac{\sin\theta\cos\theta}{d^2\mathcal{B}} + \frac{\sin\theta\cos\theta}{\mathcal{R}} \\ -\frac{\sin\theta\cos\theta}{d^2\mathcal{B}} + \frac{\sin\theta\cos\theta}{\mathcal{R}} & \frac{\cos^2\theta}{d^2\mathcal{B}} + \frac{\sin^2\theta}{\mathcal{R}} \end{bmatrix} \tag{10}$$

where $\mathcal{B} = \mathsf{CRLB}^{(\hat{\theta})}$ and $\mathcal{R} = \mathsf{CRLB}^{(\hat{d})}$ have been defined to shorten the notation. The determinant of the FIM $\tilde{\mathbf{J}}(\tilde{\mathbf{p}})$ is given by $\det(\tilde{\mathbf{J}}(\tilde{\mathbf{p}})) = 1/(d^2\,\mathcal{B}\,\mathcal{R})$. Then, the corresponding inverse FIM $\tilde{\mathbf{J}}^{-1}(\tilde{\mathbf{p}})$ is

$$\tilde{\mathbf{J}}^{-1}(\tilde{\mathbf{p}}) = d^2\,\mathcal{B}\,\mathcal{R} \times \begin{bmatrix} \frac{\cos^2\theta}{d^2\mathcal{B}} + \frac{\sin^2\theta}{\mathcal{R}} & \frac{\sin\theta\cos\theta}{d^2\mathcal{B}} - \frac{\sin\theta\cos\theta}{\mathcal{R}} \\ \frac{\sin\theta\cos\theta}{d^2\mathcal{B}} - \frac{\sin\theta\cos\theta}{\mathcal{R}} & \frac{\sin^2\theta}{d^2\mathcal{B}} + \frac{\cos^2\theta}{\mathcal{R}} \end{bmatrix} \tag{11}$$

whose trace is

$$\mathrm{tr}\left(\tilde{\mathbf{J}}^{-1}(\tilde{\mathbf{p}})\right) = \left(\cos^2\theta + \sin^2\theta\right)\left(\mathcal{R} + d^2\mathcal{B}\right) \tag{12}$$

allowing to write the PEB in (6) as

$$\mathsf{PEB} = \sqrt{\mathcal{R} + d^2\,\mathcal{B}}. \tag{13}$$

As evident from (13), the bearing error has a greater impact on the positioning accuracy as the distance d increases.

TABLE I
SIMULATION PARAMETERS

Parameter	Symbol	Value
Transmitted power	P_{T}	23 dBm
Antenna element gain	G	3 dB
Number of antennas	N_{ant}	4, 8
Frequency	f_{c}	5.9 GHz
Receiver noise figure	F	6 dB
Available channel bandwidth	$--$	40 MHz
SCS	Δf	15, 30, 60 kHz
MCS	$--$	5, 23
Packet size	$--$	350, 1000 bytes
Packet generation interval	$--$	100 ms
# of OFDM symbols	M	14
Average vehicle speed	$--$	70 km/h
STD of vehicle speed	$--$	7 km/h
Vehicle density	$--$	$10 \div 50$ veh/km
Target RCS	σ	10 m^2

TABLE II
RESULTING NUMBER OF SUBCARRIERS AND TRANSMISSION BANDWIDTH FOR THE CONFIGURATIONS CONSIDERED IN SIMULATIONS

Packet	MCS	N	Δf [kHz]	W [MHz]
350	5	480	15	7.2
350	5	480	30	14.4
350	5	480	60	28.8
350	23	120	15	1.8
350	23	120	30	3.6
350	23	120	60	7.2
1000	23	240	15	3.6

III. NUMERICAL RESULTS

We analyzed the positioning performance limits through the open-source simulator WiLabV2Xsim [20]. The simulator allows to evaluate the SINR by accounting for multiple vehicles and the resource allocation policies of 5G NR-V2X sidelink. In particular, we considered Mode 2 (autonomous allocation) [4] where every vehicle autonomously selects the time and frequency resource elements to accommodate the data packet. A highway scenario is assumed, with three lanes in each direction. In this case, the line of sight (LOS) assumption characteristic of the model in (2) can be considered as fulfilled with good approximation for the closest target, which is the most important to detect for safety reasons (candidate for collision). The SINR values obtained from the simulator are adopted to evaluate (3) and (5). Thus, this approach provides benchmark performance for any signal processing scheme implementation, considering realistic conditions in terms of interference, 5G parameters and protocol. In the regions where the performance appears interesting, further investigations also considering non-idealities not captured by this approach, such as multipath propagation, might be realized to understand how far real results are from the bound. Simulation parameters are reported in Tab. I.

Fig. 2 shows the comparison between the empirical CDFs of the root CRLB for range and bearing estimation, considering $d = 20$ m and $\theta = 0$. Two different tests were performed: *i)* varying the packet size and the vehicle density, with MCS 23 and $\Delta f = 15$ kHz (Figs. 2(a) and 2(b)); *ii)* varying the MCS and SCS, considering packets of 350 bytes and a vehicle density of 50 veh/km, (Figs. 2(c) and 2(d)). The corresponding number of subcarriers N for each configuration is reported in Tab. II.

Regarding the first test, an increment in the vehicle density produces a worsening of the performance both for range and bearing estimation, due to higher interference.

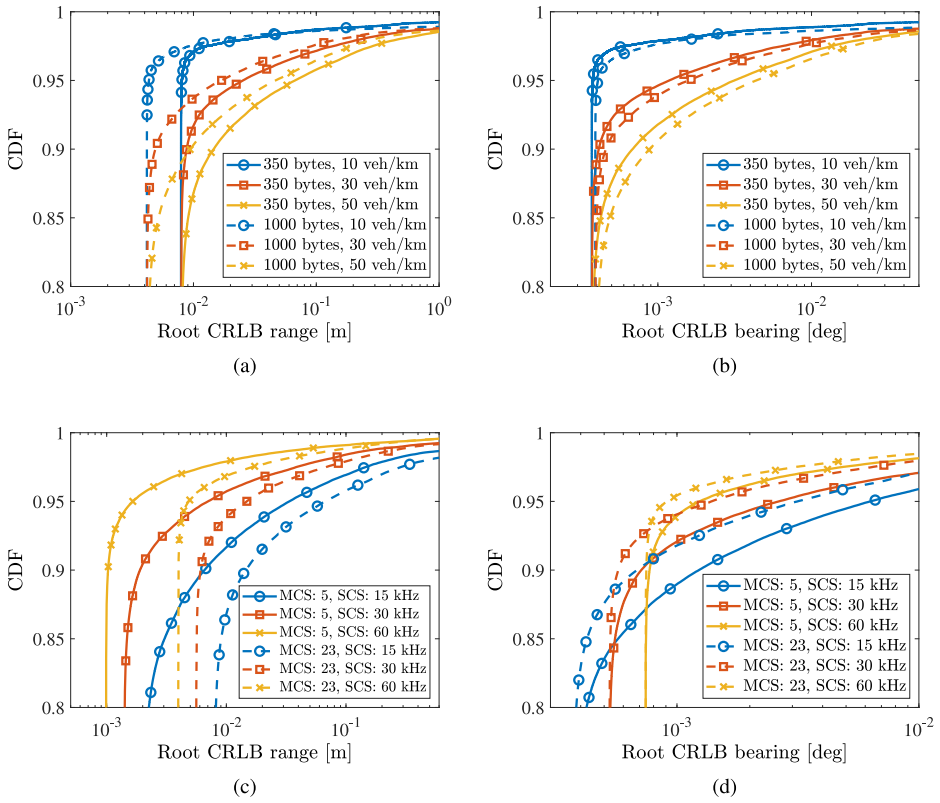

Fig. 2. Empirical CDFs for range estimation (Figs. (a) and (c)) and bearing estimation (Figs. (b) and (d)) at $d = 20$ m and $\theta = 0$, for $N_{\text{ant}} = 4$. Figs. (a) and (b) are obtained varying packet size and vehicle density, with MCS 23 and $\Delta f = 15$ kHz. Figs. (c) and (d) are obtained varying MCS and Δf, with packets of 350 bytes and 50 veh/km.

Moreover, Fig. 2(a) shows an enhancement in range estimation performance as the packet size increases. This improvement is due to the larger bandwidth resulting from a greater number of subcarriers, which helps to mitigate the inter-vehicle interference, and leads to a significant gain on the CRLB. Differently, for bearing estimation, no differences are experienced with the packet size in the absence of interference (see the vertical asymptote in Fig. 2(b)); however, when considering interference, the increase of the bandwidth due to larger packets leads to higher interference, as it can be seen in Fig. 2(b), where the gap between the solid and the dashed lines grows as the vehicle density (and thus interference) increases. Hence, the packet size has an opposite impact on range and bearing estimation only when in the presence of interference.

The second test shows the impact of MCS and SCS. Fig. 2(c) shows a significant improvement for the range estimation when a higher value of SCS is used, once again thanks to the bandwidth enlargement. This is advantageous even when the interference becomes significant; for the same reason, it is preferable to use a lower value of MCS. Results change when considering the bearing estimation performance in Fig. 2(d). In the absence of interference (vertical asymptotes), larger SCS is not beneficial, due to the larger noise accumulated with a bandwidth $N\Delta f$ in the denominator of the SINR; whereas, when considering interference, the behavior is similar to that highlighted for range estimation, and larger SCS improves the performance. In fact, the larger SCS leads to a shorter packet, thus limiting interference due to less chance of collisions. As before, higher MCS can limit the effect of interference, while the choice of MCS has no impact on the performance in the interference-free case.

Fig. 3 shows the two-dimensional maps representing the PEB obtained according to (13), thus showing the joint effect of range and bearing estimates and the spatial distribution of the error for different configurations. Each point on the map is derived considering the 95-percentile of the root CRLB for range and bearing estimation. Two cases are considered, i.e., $N_{\text{ant}} = 4$ and $N_{\text{ant}} = 8$. It can be noted that the localization capability at the outermost angles (near $\theta = \pm\pi/2$) is compromised due to the adoption of an ULA. In the considered setup, larger SCS improves the localization performance, especially thanks to the increased ranging resolution. In fact, since only small distances from the target are taken into account here, the impact of bearing estimation is less significant, according to (13). The strong improvement of using a higher number of antenna elements composing the ULA is highlighted, by comparing the maps obtained with 4 antennas (Figs. 3(a)-3(b)) and those with 8 (Figs. 3(c)-3(d)).

IV. Conclusion

We proposed a framework for evaluating device-free positioning performance limits for JCS based on V2X sidelink. To this aim, we provided the error bounds considering 5G NR-V2X technology, which are the benchmark performance of practical localization schemes. System-level simulations are performed accounting for multi-user interference and varying the physical and radio access parameters. Results show that, when considering interference, the packet size has an opposite impact on range and bearing estimation; similarly, SCS and MCS affect differently range and bearing estimates depending on the configuration. However, for close targets, maximizing

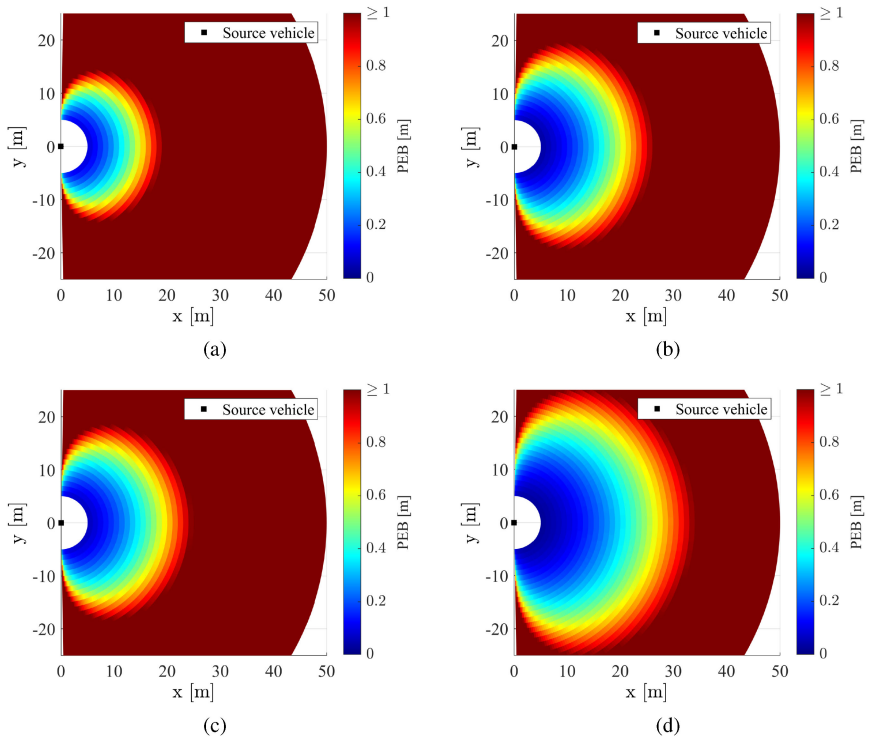

Fig. 3. PEB 2D maps for different configurations of SCS, considering a packet size of 350 bytes, MCS 23 and a vehicle density of 50 veh/km. First row: 4 antennas; second row: 8 antennas. (a), (c): $\Delta f = 15$ kHz. (b), (d): $\Delta f = 60$ kHz.

the ranging accuracy leads to the best performance in terms of positioning. The model and results of this letter can drive the design of future JCS systems leveraging V2X sidelink.

REFERENCES

[1] T. Wild, V. Braun, and H. Viswanathan, "Joint design of communication and sensing for beyond 5G and 6G systems," *IEEE Access*, vol. 9, pp. 30845–30857, 2021.

[2] C. B. Barneto, S. D. Liyanaarachchi, M. Heino, T. Riihonen, and M. Valkama, "Full duplex radio/radar technology: The enabler for advanced joint communication and sensing," *IEEE Wireless Commun.*, vol. 28, no. 1, pp. 82–88, Feb. 2021.

[3] R. Chattopadhyay and C.-K. Tham, "Joint sensing and processing resource allocation in vehicular ad-hoc networks," *IEEE Trans. Intell. Veh.*, vol. 8, no. 1, pp. 616–627, Jan. 2023.

[4] M. H. C. Garcia et al., "A tutorial on 5G NR V2X communications," *IEEE Commun. Surveys Tuts.*, vol. 23, no. 3, pp. 1972–2026, 3rd Quart., 2021.

[5] A. Kakkavas, M. H. C. Garcia, R. A. Stirling-Gallacher, and J. A. Nossek, "Multi-array 5G V2V relative positioning: Performance bounds," in *Proc. IEEE Global Commun. Conf.*, 2018, pp. 206–212.

[6] Y. Ge, M. Stark, M. F. Keskin, F. Hofmann, T. Hansen, and H. Wymeersch, "Analysis of V2X Sidelink positioning in sub-6 GHz," in *Proc. 3rd Int. Symp. Joint Commun. Sens.*, 2023, pp. 1–6.

[7] N. Decarli, A. Guerra, C. Giovannetti, F. Guidi, and B. M. Masini, "V2X sidelink localization of connected automated vehicles," *IEEE J. Select. Areas Commun.*, vol. 42, no. 1, pp. 120–133, Jan. 2024.

[8] W. U. Khan, F. Jameel, N. Kumar, R. Jäntti, and M. Guizani, "Backscatter-enabled efficient V2X communication with non-orthogonal multiple access," *IEEE Trans. Veh. Technol.*, vol. 70, no. 2, pp. 1724–1735, Feb. 2021.

[9] S. Bartoletti, N. Decarli, and B. M. Masini, "Sidelink 5G-V2X for integrated sensing and communication: The impact of resource allocation," in *Proc. IEEE Int. Conf. Commun. Workshops*, 2022, pp. 79–84.

[10] C. Liu et al., "Learning-based predictive beamforming for integrated sensing and communication in vehicular networks," *IEEE J. Select. Areas Commun.*, vol. 40, no. 8, pp. 2317–2334, Aug. 2022.

[11] C. Baquero Barneto et al., "Full-duplex OFDM radar with LTE and 5G NR waveforms: Challenges, solutions, and measurements," *IEEE Trans. Microw. Theory Tech.*, vol. 67, no. 10, pp. 4042–4054, Oct. 2019.

[12] C. Campolo et al., "Enhancing the 5G-V2X Sidelink autonomous mode through full-duplex capabilities," in *Proc. 95th IEEE Veh. Techn. Conf. (VTC-Spring)*, 2022, pp. 1–6.

[13] L. Pucci, E. Paolini, and A. Giorgetti, "System-level analysis of joint sensing and communication based on 5G new radio," *IEEE J. Select. Areas Commun.*, vol. 40, no. 7, pp. 2043–2055, Jul. 2022.

[14] S. M. Kay, *Fundamentals of Statistical Processing: Estimation Theory*, vol. 1, Hoboken, NY, USA: Prentice-Hall, 1993.

[15] M. F. Keskin, V. Koivunen, and H. Wymeersch, "Limited feedforward waveform design for OFDM dual-functional radar-communications," *IEEE Trans. Signal Process.*, vol. 69, pp. 2955–2970, Apr. 2021.

[16] A. Bazzi, A. O. Berthet, C. Campolo, B. M. Masini, A. Molinaro, and A. Zanella, "On the design of sidelink for cellular V2X: A literature review and outlook for future," *IEEE Access*, vol. 9, pp. 97953–97980, 2021.

[17] P. Gertzell et al., "5G multi-BS positioning with a single-antenna receiver," in *Proc. IEEE 31st Annu. Int. Symp. Pers., Indoor Mobile Radio Commun.*, 2020, pp. 1–5.

[18] Z. Abu-Shaban, H. Wymeersch, T. Abhayapala, and G. Seco-Granados, "Single-anchor two-way Localization bounds for 5G mmWave systems," *IEEE Trans. Veh. Technol.*, vol. 69, no. 6, pp. 6388–6400, Jun. 2020.

[19] D. B. Jourdan, D. Dardari, and M. Z. Win, "Position error bound for UWB localization in dense cluttered environments," *IEEE Trans. Aerosp. Electron. Syst.*, vol. 44, no. 2, pp. 613–628, Apr. 2008.

[20] V. Todisco, S. Bartoletti, C. Campolo, A. Molinaro, A. O. Berthet, and A. Bazzi, "Performance analysis of sidelink 5G-V2X mode 2 through an open-source simulator," *IEEE Access*, vol. 9, pp. 145648–145661, 2021.

Open Access funding provided by 'Consiglio Nazionale delle Ricerche-CARI-CARE-ITALY' within the CRUI CARE Agreement